The effect of seawater salinity on sea spray aerosol production

J. Zinke[1,2], E. D. Nilsson[1,2], P. Zieger[1,2,]and M. E. Salter[1,2]

[1]Department of Environmental Sciences, Stockholm University, Stockholm, Sweden
[2]Bolin Centre for Climate Research, Stockholm University, Stockholm, Sweden

Key Points:

- The concentrations and size distributions of sea spray aerosol depend on the seawater salinity and temperature
- Three salinity regimes with distinct patterns in particle number, volume and surface bubble spectra were identified
- A parameterization has been derived for total sea spray particle number and effective radius as a function of water temperature and salinity

Corresponding author: E. Douglas Nilsson, douglas.nilsson@aces.su.se

Corresponding author: Julika Zinke, julika.zinke@aces.su.se

Abstract

To improve our understanding of the impact of sea spray aerosols (SSA) on the Earth's climate, it is critical to understand the physical mechanisms which determine the size-resolved sea spray aerosol source. Of the factors affecting SSA emissions, seawater salinity has perhaps received the least attention in the literature and previous studies have produced conflicting results. Here, we present a series of laboratory experiments designed to investigate the role of salinity on aerosol production from artificial seawater using a continuous plunging jet. During these experiments, the aerosol and surface bubble size distributions were monitored while the salinity was decreased from 35 to $0\,\mathrm{g\,kg^{-1}}$. Three distinct salinity regimes were identified: 1) A high salinity regime, 10-35 $\mathrm{g\,kg^{-1}}$, where decreasing salinity only resulted in minor reductions in particle number emissions but significant reductions in particle volume; 2) an intermediate salinity regime, 5-10 $\mathrm{g\,kg^{-1}}$, with a local maximum in particle number; 3) a low salinity regime, $< 5\ \mathrm{g\,kg^{-1}}$, characterized by a rapid decrease in particle number as salinity decreased and dominated by small particles and larger bubbles. We discuss the implications of our results through comparison of the size-resolved aerosol flux and the surface bubble population at different salinities. Finally, by varying the seawater temperature at three specific salinities we have also generated a simple parameterization of the particle number concentration and effective radius as a function of seawater temperature and salinity that can be used to estimate the sea spray aerosol flux in low salinity regions like the Baltic Sea.

1 Introduction

Along with mineral dust, sea spray aerosol (SSA) is the major component of Earth's natural aerosol in terms of mass and has the potential to influence the Earth's climate system by scattering incoming solar radiation and acting as cloud condensation nuclei (e.g. Schwartz, 1996; Murphy et al., 1998; Quinn et al., 1998). These impacts are strongly influenced by the number and size of the sea spray aerosol particles. Therefore, understanding the physical mechanisms which determine the source strength of sea spray aerosol as a function of particle size is critical if we are to determine the influence of sea spray aerosol on climate. Along with wind speed, the water temperature, salinity, and the physico-chemical and biological state of the ocean have been shown to influence the production of sea spray aerosol. Of these variables salinity has perhaps received the least attention in the literature and previous studies that have attempted to determine the effect of seawater salinity on sea spray aerosol production have produced conflicting results.

The main studies concerned with the effect of salinity on the production flux of sea spray aerosol have been conducted using laboratory sea spray simulation systems where bubbles have been generated from artificial seawater utilizing frits (e.g. Mårtensson et al., 2003; Tyree et al., 2007; Park et al., 2014) or from NaCl solutions utilizing plunging jet systems (e.g. Zábori et al., 2012; May et al., 2016). An overview of previous experiments can be found in Table S1. It is important to note that the bubble size distributions generated with frits are very sensitive to the characteristics of the specific frits used and likely differ markedly from the bubble size distributions found under oceanic breaking waves (e.g. Collins et al., 2014). In contrast plunging jet systems have been shown to generate bubble size distributions more similar to breaking waves (Hultin et al., 2010; Stokes et al., 2013) as well as sea spray aerosol that is chemically more similar to that found over breaking waves (Collins et al., 2014; Facchini et al., 2008).

In terms of the dependence of the SSA production flux on salinity, Mårtensson et al. (2003) reported an increase in the SSA production flux as the salinity was increased, which is most evident for particles with dry diameter $D_p > 0.1\,\mu\mathrm{m}$. For particles with $D_p < 0.1\,\mu\mathrm{m}$ there was little difference in the particle number between the experiments with seawater salinity 9.2 and 33 $\mathrm{g\,kg^{-1}}$. However, the aerosol size distribution exhibited a slight shift to larger particle sizes at the higher salinity. Both Tyree et al. (2007) and Zábori et al.

(2012) also observed a shift to larger particle sizes when the salinity was increased from 1 to 10 $g\,kg^{-1}$ and 0 to 15 $g\,kg^{-1}$, respectively. However, neither Park et al. (2014) nor May et al. (2016) observed such a shift in particle size with increasing salinity.

More recently, Nilsson et al. (2021) compared the observed eddy covariance aerosol fluxes in the Baltic Sea at salinity $\sim 8\ g\,kg^{-1}$ with the parameterizations by Mårtensson et al. (2003) and Salter et al. (2015) and concluded that the observed number emission fluxes agreed with the parameterizations when they were corrected by the cube root of the salinity S. This suggests that the mass emissions are proportional to the salinity.

Despite these rather conflicting findings, one similarity across many of the previous studies is that the SSA production flux is most sensitive to changes at lower salinities ($< 10\ g\,kg^{-1}$) (Mårtensson et al., 2003; Tyree et al., 2007; Zábori et al., 2012). This is not surprising given the significant changes in bubble coalescence that have been noted across this range of salinities (Lewis & Schwartz, 2004; Craig et al., 1993). In essence, bubble coalescence is reduced in seawater compared to freshwater which results in the former containing more small bubbles than the latter (e.g. Slauenwhite & Johnson, 1999). The reason for this difference has been attributed to the existence of electrolytes in seawater and recent evidence appears to support this view (Katsir et al., 2015). Critically, this range in salinity is interesting from the perspective of modeling the production of SSA from low salinity waters such as the central and northern Baltic Sea where the salinity is lower than $10\ g\,kg^{-1}$.

Other examples of low to moderate salinity seawaters are the Black Sea (14-19 $g\,kg^{-1}$) and the Hudson Bay and Strait (26-31 $g\,kg^{-1}$). Indeed, these regions along with areas such as Baffin Bay (30-32 $g\,kg^{-1}$ in summer), the Labrador Sea (30-34 $g\,kg^{-1}$) and other Arctic and Antarctic surface waters are predicted to become less saline with climate change (Lavoie et al., 2013; Kniebusch et al., 2019). To this end, the intention of this study was to investigate the production of SSA from artificial seawater with salinities between 0 and 35 $g\,kg^{-1}$ using a well-characterized plunging jet sea spray chamber. Given the aforementioned transition in bubble coalescence behavior between salinities 0 and 10 $g\,kg^{-1}$ particular focus was placed on these lower salinities. Alongside measurements of the size and number of SSA produced, we have also measured the bubble size distribution at the air-water interface of the sea spray chamber with the aim of understanding the processes that link changing salinity and the size-resolved aerosol flux.

2 Materials and Methods

2.1 The Sea Spray Chamber

Sea spray aerosols were generated in a temperature-controlled sea spray generation chamber using a plunging jet. This system has been described in detail by Salter et al. (2014) and details are provided in the supplementary information.

2.2 Particle Size Distribution Measurements

Aerosol particle-laden air was sampled through 0.8 m of tubing, a 1 m long Nafion dryer (MD-700-36F, Perma Pure, USA), followed by another 1.9 m of tubing after which the flow was split. A condensation particle counter (CPC, MCPC 1720, Brechtel Inc., USA) with a flow rate of 0.36 $L\,min^{-1}$ situated 0.4 m behind this split was used to enumerate the total number concentration for particles with diameters > 0.01 µm. The size distribution of aerosol particles with dry electrical mobility diameters $0.015\,\mu m < D_p < 0.906\,\mu m$, distributed over 37 size bins, was measured with a custom-built differential mobility particle sizer (DMPS), consisting of a 28 cm long Vienna type differential mobility analyzer (DMA) and a condensation particle counter (CPC, MCPC 1720, Brechtel Inc., USA) with a flow rate of 0.36 $L\,min^{-1}$. A scan over all size bins was completed in 12 minutes and the measured

size distributions were inverted and multiple-charge corrected using custom-built software. The DMPS was situated 0.5 m behind the split.

An optical particle size spectrometer (OPSS) with a flow rate of 5 $\mathrm{L\,min^{-1}}$ (WELAS 2300 HP sensor and Promo LED 2000 H, Palas GmbH, Germany) was mounted 0.7 m above the sea spray chamber and measured the particle size distribution in the optical diameter size range $0.150\,\mu\mathrm{m} < \mathrm{D}_p < 10\,\mu\mathrm{m}$, distributed over 59 bins. The optical diameter measured by the OPSS depends on the wavelength-dependent refractive index of the sampled aerosol. Therefore, we have converted the measured optical diameters to volume equivalent diameters by assuming a refractive index of $m = 1.54 - 0i$ for sea salt particles, which corresponds to the value of NaCl (Abo Riziq et al., 2007). The correction was conducted using the software provided by the manufacturer (PDAnalyze, Palas GmbH, Version No 2.024). A 1.3 m long Nafion dryer (MD-700-48F, Perma Pure, USA) with a sheath flow of 10 $\mathrm{L\,min^{-1}}$ was mounted horizontally in front of the OPSS in order to reduce the humidity of the sampled air so that the measured particle diameters can be considered as dry diameter. Temperature and relative humidity were monitored with two sensors (HYTELOG-USB, B+B Thermo-Technik GmbH) mounted in front of the sampling inlets of the OPSS and DMPS system. The humidities measured in front of the DMPS and OPSS were $21.3 \pm 0.38\%$ and $17.1 \pm 0.31\%$, respectively (mean $\pm$ standard deviation for the entire experiment). Since SSA particles are typically non-spherical when dried, the diameters obtained from the DMPS and OPSS were shape corrected using a dynamic shape factor calculated according to Zieger et al. (2017). All sizing instruments were calibrated with polystyrene latex (PSL) spheres. Following all corrections, the data of the DMPS and OPSS were combined at 0.5 µm.

Aerosol sampling efficiencies were estimated with the Particle Loss Calculator Software (von der Weiden et al., 2009) and are shown in Figure S3. The losses of the larger particles measured by the OPSS were expected to be highest in the horizontally aligned Nafion dryer. The estimated losses also depend on the particle density, which is in turn dependent on how quickly the water within the particles evaporates during transit through the drier (i.e how much time the particles spend as droplets in the drier versus how much time they spend as salt crystals). Since the drying of the particles is a continuous process, we have considered a density range from that of seawater, $1000\,\mathrm{kg\,m^{-3}}$, to that of dry sea salt particles, $2017\,\mathrm{kg\,m^{-3}}$ (Zieger et al., 2017). Note, while these values provide upper and lower limits for the estimated sampling efficiency, we have not corrected the data presented in this study for any particle losses.

MATLAB software version 2019a was used to conduct statistical tests on the size distributions. The Mathworks Curve Fitting Toolbox 3.5.9, which uses the method of least squares when fitting data, was used to establish empirical relationships. All fits presented in this study are non-weighted.

2.3 Surface bubble spectra

The bubble size distribution at the water surface was determined photographically in a similar fashion to that described in Salter et al. (2014). Details can be found in the supplementary information.

2.4 Experimental Setup

The experiments were conducted with artificial seawater consisting of Sigma sea salt (Sigma Aldrich, S9883; with ionic mass ratios comparable to those in seawater: 55% $\mathrm{Cl^-}$, 31% $\mathrm{Na^+}$, 8% $\mathrm{SO_4^{2-}}$, 4% $\mathrm{Mg^{2+}}$, 1% $\mathrm{K^+}$, 1% $\mathrm{Ca^{2+}}$, < 1% other) that was dissolved in low organic carbon standard deionized water (MilliQ, > 18.2 MΩ), hereafter referred to as DIW. Previous studies have shown that there are no substantial amounts of organics in the salt (e.g. Salter et al., 2016). In order to estimate the effect of salinity on sea spray production the salinity was gradually decreased from 35 to 0 $\mathrm{g\,kg^{-1}}$ while the temperature was kept

constant at 20°C. This experiment was repeated at a higher salinity resolution in the range 10-5 g kg^{-1} where significant impacts of changing salinity on the aerosol and bubbles were expected. Each experiment started when the measured salinity had settled to a constant value. We chose to decrease the salinity rather than increase it since dilution of 100 L of artificial seawater with DIW proceeds much more quickly to steady state than the dissolution of additional salt.

In addition to the experiments conducted at a constant temperature, three temperature ramps were conducted at salinities 35 g kg^{-1}, 17 g kg^{-1} and 6 g kg^{-1} to investigate the impact of changing the water temperature on particle production at different salinities. These salinities were chosen because they are representative of the global average oceanic salinity as well as lower salinity waters such as the Black Sea and the Baltic Sea. During these temperature ramps the water temperature was slowly decreased from 30 to 0°C over a period of approximately 40 hours. Two temperature ramps were conducted at salinity 35 g kg^{-1} to examine the reproducibility of the measurements.

3 Results and Discussion

3.1 Impact of seawater salinity on particle production

By varying the amount of sea salt dissolved in DIW and measuring the particle size distribution we have probed the impact of changing salinity on particle production. Figure 1 presents the aerosol particle number, surface and volume size distributions for seawater salinities between 0 and 35 g kg^{-1}. For seawater salinities $\geq$ 15 g kg^{-1} the number size distribution had a local maximum at 146 nm and a second local maximum at 403 nm when presented in the form dN/dlogD$_p$ where N is the number of particles and D$_p$ is the volume equivalent diameter (see also Figure S4). As the seawater salinity decreased below 15 g kg^{-1} the first local maximum shifted to 66-74 nm and the second local maximum ceased to exist. When presented in the form dA/dlogD$_p$, the surface size distribution exhibited a mode that was centered around 3 µm at salinities $\geq$ 15 g kg^{-1} and shifted to 2 µm at salinities $\leq$ 15 g kg^{-1}. The magnitude of dA/dlogD$_p$ decreased notably at seawater salinities $<$ 15 g kg^{-1}. Similarly, the particle volume size distribution exhibited a mode that was centered around 5 µm at salinities $\geq$ 15 g kg^{-1}, which shifted to 3 µm for salinities $\leq$ 10 g kg^{-1} and simultaneously decreased in magnitude. Another prominent feature of the size distributions was a substantial increase in the concentration of particles <100 nm at seawater salinities 6 and 8 g kg^{-1} relative to both higher and lower seawater salinities.

A comparison to previous studies conducted by Mårtensson et al. (2003), Tyree et al. (2007), Zábori et al. (2012) and Park et al. (2014) is provided in Figure 2. Tyree et al. (2007) observed a shift to larger particle sizes from 62.5 nm to 98 nm (center of the mode) as the seawater salinity was increased from 1 to 10 g kg^{-1}. Similarly, Zábori et al. (2012) observed a shift in the center of the mode from about 142 to 225 nm as the seawater salinity was increased from 0–3 g kg^{-1} to 12–15 g kg^{-1}. Our study supports the findings of both these studies. With that said, it should be noted that Zábori et al. (2012) observed that the mean relative humidity was 43% during their experiments in the seawater salinity range 0-18 g kg^{-1}. At such high relative humidities the particles were unlikely to be dry and should not be referred to as particles at "dry diameter". Therefore, we have converted their diameters to dry diameters assuming a growth factor of 1.22 at RH=43% (Zieger et al., 2017). By doing so we have calculated dry diameters of 116 nm for the salinity range 0–3 g kg^{-1} and 184 nm for the salinity range 12–15 g kg^{-1}. These values compare reasonably well with the shift from $\sim$ 70 nm to 140 nm observed in the current study. While Tyree et al. (2007) used a frit to generate sea spray aerosols, Zábori et al. (2012) used a plunging jet. Mårtensson et al. (2003) also observed a shift in the mode diameter from 60 nm to 125 nm as seawater salinity increased. However, in this study the shift to larger sizes occurred at higher seawater salinities between 9.2 and 33 g kg^{-1}. In the current study, although we

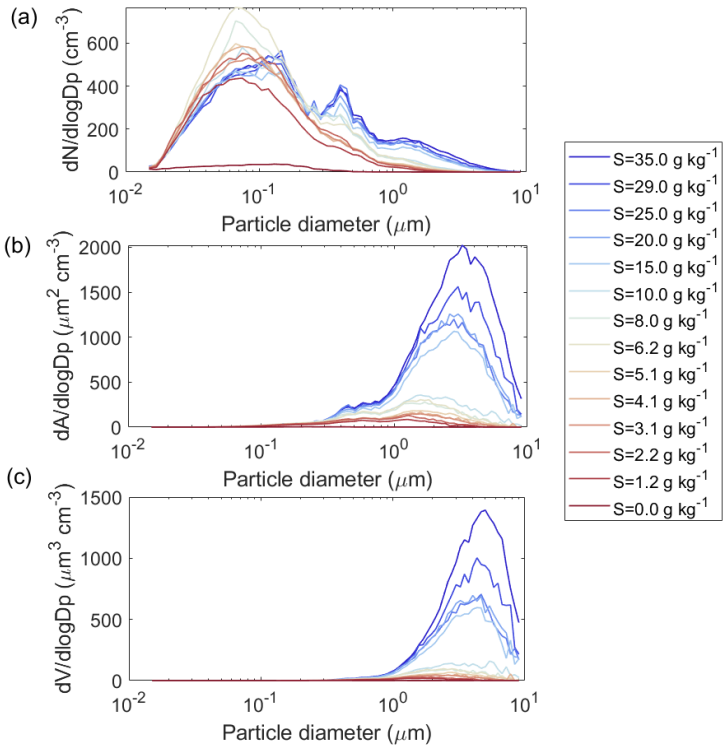

Figure 1. Mean particle (a) number size distribution, (b) surface size distribution, and (c) volume size distribution measured at different salinities at a water temperature of 20°C. The diameters are volume equivalent diameters.

observed a shift in the main particle number mode diameter with changing salinity (see Figure 1), we did not observe a monotonic increase in the main particle number mode with increasing seawater salinity which has been observed in previous studies (e.g. Tyree et al., 2007; Park et al., 2014; May et al., 2016). Since two of these previous studies used frits to produce bubbles (Tyree et al., 2007; Park et al., 2014), the bubble spectra present during their experiments were very likely different from those in experiments utilizing plunging jets (such as the current study). May et al. (2016) used multiple plunging jets and the authors make note of the shallow bubble plume which resulted. This likely impacted the bubble lifetime in this system and potentially explains the difference in their observed particle distributions compared to the current study.

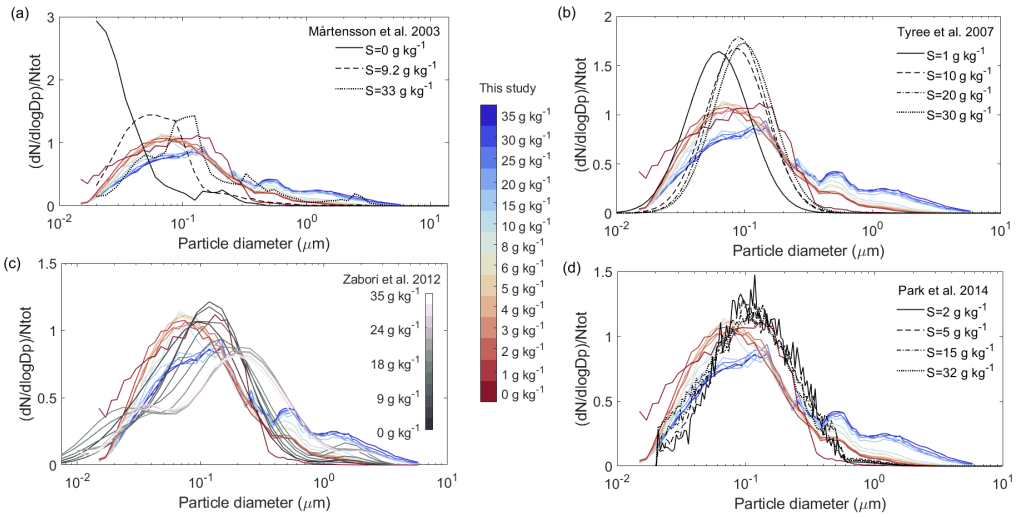

Figure 2. Comparison of the normalized size distributions for different salinities obtained from this study with the results from (a) Mårtensson et al. (2003), (b) Tyree et al. (2007), (c) Zábori et al. (2012) and (d) Park et al. (2014).

The particle size distributions presented in Figure 1 highlight that changing seawater salinity induced complex changes in the particle size distribution following bubble bursting. Therefore, in order to visualize these changes, Figure 3 presents particle number, surface and volume concentrations that were obtained by integrating over the whole size range of the combined size distributions measured by the DMPS and OPSS as well as the effective particle radius as functions of seawater salinity. Here, the effective radius r_e was calculated following Grainger et al. (1995): $r_e = \frac{3V}{A}$.

From Figure 3a, three distinct regimes can be identified, each with a different relationship between seawater salinity and integrated particle number. The first regime occurred at seawater salinities greater than 10 $g\,kg^{-1}$ where the integrated particle number decreased only gradually with decreasing seawater salinity. The second regime occurred in the salinity range 5-10 $g\,kg^{-1}$ where a peak in integrated particle number production occurred in the first set of experiments. Finally, a third regime was observed at seawater salinities <5 $g\,kg^{-1}$ where the integrated particle number decreased rapidly as seawater salinity decreased. The integrated concentrations were compared to the total number concentration measured by the CPC (see Figure S5). The measured total number concentrations exhibited the same three regimes, although shifted downward in magnitude by an average of 17% ± 2% for all salinities except 0 $g\,kg^{-1}$.

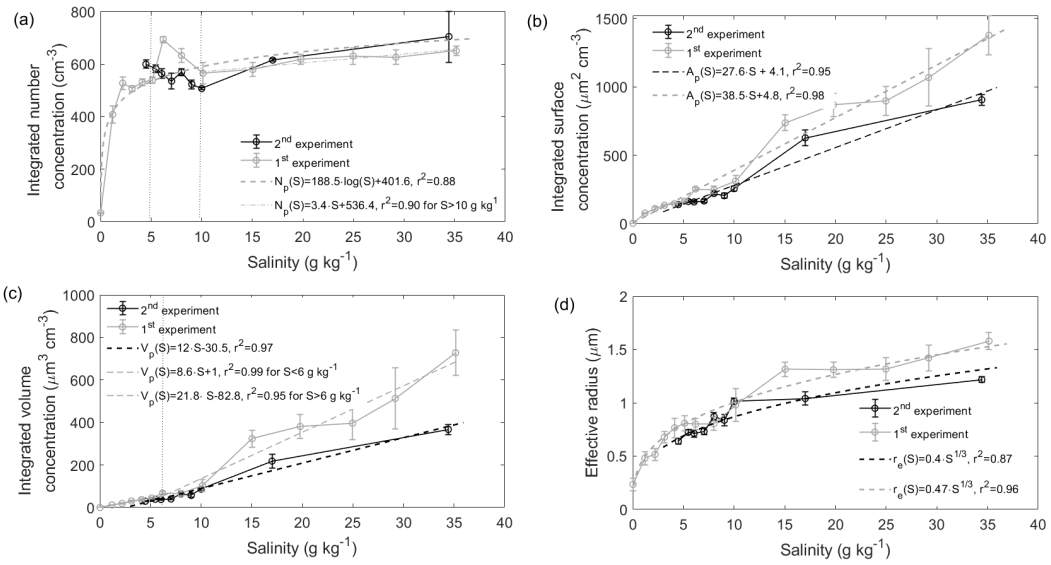

Figure 3. The impact of salinity on the (a) particle number, (b) surface, (c) volume concentration and (d) effective radius including fits. All values are presented as mean values and standard deviation. The dotted lines in panel (a) and (c) mark regimes with different relationships between seawater salinity and particle number or volume.

In order to investigate the local maxima in particle production in the seawater salinity range 5-10 g kg^{-1} more deeply, a second experiment was carried out with increased salinity resolution in this range. This experiment also showed a local maximum in particle production in this range. However, the exact salinity at which this local maximum in particle production occurred differed between the two experiments (6 g kg^{-1} for the first experiment, 4.5 g kg^{-1} for the second experiment). This suggests that some property of the seawater used in the two experiments differed. Since seawater temperature was controlled we can exclude this as a factor. Instead, it may have been that slight changes in the organic matter unintentionally present in the seawater impacted the bubble bursting process.

Zábori et al. (2012) observed a local maximum in particle number production in the salinity range 3-9 g kg^{-1} that is consistent with the increased particle production at seawater salinities 6 and 8 g kg^{-1} observed in the current study. Note that the salinity bins in Zábori et al. (2012) are wider than the steps used in the current study.
We suspect that the observed changes in particle number with salinity result from changes in the bubble spectra that are discussed in section 3.2.

Both particle surface and volume decreased monotonically as seawater salinity decreased (Figures 3b and c). The strong dependence of both particle surface and volume concentration on seawater salinity likely results from the lower ion concentrations and subsequent lower solute concentrations of the dried particles (assuming the initial droplet was the same size) as seawater salinity decreased as previously hypothesized by Mårtensson et al. (2003) and Slade et al. (2010). Although Mårtensson et al. (2003) only measured the impact of seawater salinity on particle production at three different salinities, they also observed monotonically decreasing particle volume with decreasing salinity. Closer inspection of Figure 3c reveals two distinct salinity regimes. At seawater salinities $\geq$ 6 g kg^{-1} the particle volume concentration decreased more rapidly as salinity decreased compared to salinities lower than 6 g kg^{-1}. The effective radius r_e (Figure 3d) decreased non-linearly as seawater salinity decreased.

In order to parameterize the effect of salinity on sea spray aerosol production, we have attempted to describe the integrated particle number concentration as a function of seawater salinity by defining the following empirical equation

$$N_p = 188.5\ \mathrm{cm^{-3}} \cdot \log(S) + 401.6\ \mathrm{cm^{-3}} \tag{1}$$

where N_p denotes the particle number concentration, S denotes the salinity of the water and log is the common logarithm. As is clear from Figure 3a this empirical relationship does not account for the local maxima in particle production we observed at seawater salinities between 5 and 10 $\mathrm{g\,kg^{-1}}$ despite being a reasonable fit to the data at other seawater salinities (r^2=0.88, which describes the goodness of fit). This suggests that the local maximum is caused by processes other than the overall gradual change.

For salinities $\geq$10 $\mathrm{g\,kg^{-1}}$ the relationship between seawater salinity and particle production can be described with the empirical linear equation

$$N_p = 3.4\ \mathrm{cm^{-3}\,kg_{water}\,g_{salt}^{-1}} \cdot S + 536.4\ \mathrm{cm^{-3}},\ r^2 = 0.90 \tag{2}$$

for the first experiment. The second experiment has only three data points in this range, but indicates a linear relationship similar to that in the first experiment.

For the two distinct regimes observed in the particle volume, we have defined the following empirical relationships to describe the dependence of particle volume on seawater salinity:

$$V = k \cdot S + m \tag{3}$$

where k=8.6 $\mathrm{\mu m^3\,cm^{-3}\,kg_{water}\,g_{salt}^{-1}}$ (95% confidence bounds: 7.6 $\mathrm{\mu m^3\,cm^{-3}\,kg_{water}\,g_{salt}^{-1}}$, 9.6 $\mathrm{\mu m^3\,cm^{-3}\,kg_{water}\,g_{salt}^{-1}}$ and m=1 $\mathrm{\mu m^3\,cm^{-3}}$ (95% confidence bounds: -2.18 $\mathrm{\mu m^3\,cm^{-3}}$, 4.08 $\mathrm{\mu m^3\,cm^{-3}}$) for S<6 $\mathrm{g\,kg^{-1}}$ (r^2=0.99) and k=21.8 $\mathrm{\mu m^3\,cm^{-3}\,kg_{water}\,g_{salt}^{-1}}$ (95% confidence bounds: 17.2 $\mathrm{\mu m^3\,cm^{-3}\,kg_{water}\,g_{salt}^{-1}}$, 26.5 $\mathrm{\mu m^3\,cm^{-3}\,kg_{water}\,g_{salt}^{-1}}$ and m=-82.8 $\mathrm{\mu m^3\,cm^{-3}}$ (95% confidence bounds: -181.1 $\mathrm{\mu m^3\,cm^{-3}}$, 15.4 $\mathrm{\mu m^3\,cm^{-3}}$) for S$\geq$6 $\mathrm{g\,kg^{-1}}$ (r^2=0.95) for the first experiment. For the second experiment k=12 $\mathrm{\mu m^3\,cm^{-3}\,kg_{water}\,g_{salt}^{-1}}$ (95% confidence bounds: 10.2 $\mathrm{\mu m^3\,cm^{-3}\ kg_{water}\,g_{salt}^{-1}}$, 13.8 $\mathrm{\mu m^3\,cm^{-3}\,kg_{water}\,g_{salt}^{-1}}$ and m=-30.5 $\mathrm{\mu m^3\,cm^{-3}}$ (95% confidence bounds: -56.5 $\mathrm{\mu m^3\,cm^{-3}}$, -4.5 $\mathrm{\mu m^3\,cm^{-3}}$) for S$\geq$6 $\mathrm{g\,kg^{-1}}$ (r^2=0.97).

The linear relationship between V and S suggests that the mass flux is directly proportional to the salt mass in the water as indicated by Mårtensson et al. (2003) and Nilsson et al. (2021). The difference in dV/dS suggests that two different particle formation processes may have dominated above and below 6 $\mathrm{g\,kg^{-1}}$.

The effective radius appears to be directly proportional to the cube root of the seawater salinity as follows:

$$r_e = \alpha \cdot S^{1/3} \tag{4}$$

where α is a proportionality constant with units of $\mathrm{m\,kg_{water}^{1/3}\,g_{salt}^{-1/3}}$ if the r_e is in units of m and S is in units of $\mathrm{g_{salt}\,kg_{water}^{-1}}$. For our first experiment $\alpha = 0.47 \cdot 10^{-6}\ \mathrm{m\,kg_{water}^{1/3}\,g_{salt}^{-1/3}}$ (95% confidence bounds: $0.45 \cdot 10^{-6}\ \mathrm{m\,kg_{water}^{1/3}\,g_{salt}^{-1/3}}$, $0.49 \cdot 10^{-6}\ \mathrm{m\,kg_{water}^{1/3}\,g_{salt}^{-1/3}}$; r^2=0.96) while for our second experiment $\alpha = 0.40 \cdot 10^{-6}\ \mathrm{m\,kg_{water}^{1/3}\,g_{salt}^{-1/3}}$ (95% confidence bounds: $0.38 \cdot 10^{-6}\ \mathrm{m\,kg_{water}^{1/3}\,g_{salt}^{-1/3}}$, $0.43 \cdot 10^{-6}\ \mathrm{m\,kg_{water}^{1/3}\,g_{salt}^{-1/3}}$; r^2=0.87). These fits are consistent with particle formation where the particle mass M_p is proportional to seawater salinity:

$$S \propto M = V \cdot \rho = \rho \frac{4\pi}{3} r^3 = \rho \frac{\pi}{6} D_p^3 \tag{5}$$

3.2 Dependence of the surface bubble spectra on seawater salinity

Figure 4a presents the bubble density as a function of the bubble film radius for the measured range of salinities in the field of view. As the the water salinity decreased there was

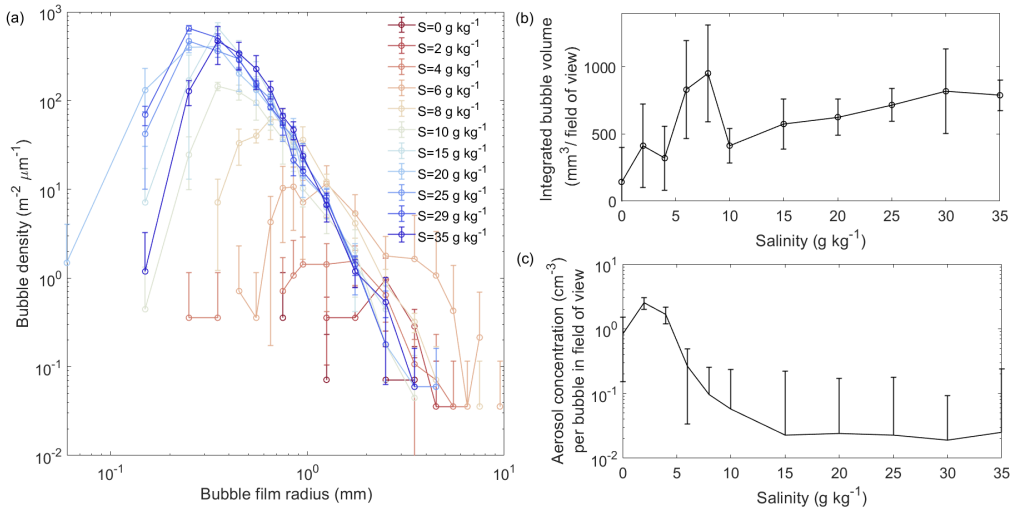

Figure 4. The impact of salinity on (a) the surface bubble density versus bubble film radius, (b) the integrated bubble volume and (c) the number of particles produced per bubble per field of view. All values are presented as mean values and standard deviation that were determined by averaging across a number of images at each salinity.

a shift toward larger bubble sizes and a decrease in bubble number density, particularly for bubbles < 1 mm peaking at a bubble radius of about 0.3-0.4 mm. The experiment conducted at a salinity of 6 g kg^{-1} exhibited higher bubble densities at bubble radii > 1 mm compared to all other salinities which otherwise exhibited a monotonic decrease in bubble density for bubbles with radii larger than 1 mm. The change in the bubble spectra as a function of salinity is more clearly demonstrated in Figure 4b, where we can see that the dependence of the integrated surface bubble volume on salinity exhibits similar behavior to the dependence of aerosol particle number on salinity (e.g. Figure 1a). That is, as the salinity decreased from 35 to 10 g kg^{-1} the surface bubble volume was nearly constant with salinity. Then, as the salinity decreased from 10 to 5 g kg^{-1}, a local maximum in bubble volume was observed. Finally, as the salinity decreased below 5 g kg^{-1} a rapid decrease in the surface bubble volume was observed. A similar decrease in the bubble concentration with decreasing salinity that is presented in Figure 4a has been reported in several previous studies. A summary of these studies is given in Lewis and Schwartz (2004). Many of these investigators (e.g. Marrucci & Nicodemo, 1967; Monahan & Zietlow, 1969; Carey et al., 1993; Cartmill & Su, 1993; Asher et al., 1997; Slauenwhite & Johnson, 1999) reported a higher number of smaller bubbles with radii < 1 mm in seawater than in freshwater which is consistent with our bubble size distribution. The higher abundance of smaller bubbles in seawater than in freshwater has been attributed to coalescence inhibition and an increased break-up of bubbles in seawater (e.g. Lessard & Zieminski, 1971; Slauenwhite & Johnson, 1999; Lewis & Schwartz, 2004). The inhibition of coalescence in seawater relative to freshwater has been attributed to the different electrolytic properties of fresh- versus seawater. The transition in bubble coalescence has been observed to happen in the salinity range 0 to 10 g kg^{-1} (Lessard & Zieminski, 1971; Craig et al., 1993) which is in agreement with the observations in the current study. Notably, previous studies (Marrucci & Nicodemo, 1967; Lessard & Zieminski, 1971; Drogaris & Weiland, 1983; Craig et al., 1993; Carey et al., 1993) have observed that bubble coalescence is significantly reduced at ionic strengths in the range 0.1-0.2 mol kg$^{-1}_{\text{seawater}}$ which corresponds to salinities between 5 and 10 g kg^{-1}. This agrees well with the peak in particle concentrations and bubble volume observed in the current study. Inline with our observations, this suggests that in regions with salinities > 10 g kg^{-1}

(e.g. the Western Baltic Kattegat, Black Sea or Hudson Bay) SSA production is likely to differ only marginally from the major oceans.

If we had imaged the entire surface of the water generating particles during our experiments we could have combined our measurements of the surface bubble number with our particle measurements to provide an estimate of the impact of salinity on the amount of particles produced per bubble. However, since our photographs cover only a fraction of the water surface, that is located close to the plunging jet, and the bubble density declines toward the edges of the sea spray tank to avoid wall effects on the bubble spectra (see Figure S2), it was not possible to estimate the total amount of bubbles at the water surface at any one time. As such, we were not able to provide such an estimate. Instead, we have estimated the number of particles produced per bubble in the area imaged (Figure 4c) to provide an estimate of the rate of change of the number of particles per bubble with varying salinity. These estimates indicate that the number of particles produced per bubble was approximately constant for S$> 10\,\mathrm{g\,kg^{-1}}$. In contrast, as the salinity decreased below 10 $\mathrm{g\,kg^{-1}}$ the number of particles produced per bubble increased rapidly with decreasing salinity reaching a maximum at a salinity of $\sim 2\,\mathrm{g\,kg^{-1}}$. The transition regime at salinities 5-10 $\mathrm{g\,kg^{-1}}$ that was so evident in both particle number (Figure 1) and bubble volume (Figure 4c) also exhibits notably different behavior for this metric. One possible explanation for the occurrence of this transition regime is a rapid change in the surface bubble size distribution from the predominance of many small bubbles at higher salinities, to the predominance of fewer larger bubbles at lower salinities.

The number of jet drops and film drops produced when a bubble bursts depends on the bubble size (Lewis & Schwartz, 2004). Bubbles with radii > 1 mm tend to produce more film drops while bubbles < 1 mm produce more jet drops (Lewis & Schwartz, 2004). As such, our observation that more sub-millimeter bubbles were present at salinities $> 10\,\mathrm{g\,kg^{-1}}$ likely coincided with an increased production of jet drops. Since we observed no notable changes in super-millimeter bubble density we conclude that film drop emissions were less impacted by changes in salinity than jet drops, which is in line with the observations of Harb and Foroutan (2019). Since jet drops tend to expel super-micron particles (Lewis & Schwartz, 2004), a higher proportion of jet drops will shift the particle size distribution mode to larger particles. This agrees well with the shift to larger particle sizes for salinities $> 10\,\mathrm{g\,kg^{-1}}$ that we observed. However, it is important to note that other studies (e.g. Wang et al., 2017) have observed that a substantial fraction of sub-micrometer particles can also be produced from jet drops.

Figure 5 presents our bubble size spectra at salinity 0 and 35 $\mathrm{g\,kg^{-1}}$ alongside those of Harb and Foroutan (2019), who used a plunging sheet of water to entrain air, and Salter et al. (2014), who used the same experimental setup as that used in the current study. All of these experiments were conducted at temperatures of around 20°C. The bubble size distribution obtained in the current study at 35 $\mathrm{g\,kg^{-1}}$ agrees fairly well with the bubble size distribution measured by Harb and Foroutan (2019), whereas we observe considerably fewer bubbles at all sizes for salinity 0 $\mathrm{g\,kg^{-1}}$ than Harb and Foroutan (2019). In the observations made by Salter et al. (2014) at 35 $\mathrm{g\,kg^{-1}}$, fewer bubbles of all sizes were present than in the current study. This is surprising given that Salter et al. (2014) used the same experimental set-up used in the current study. Further, Salter et al. (2014) observed slightly higher particle concentrations than those obtained in the current study suggesting that, if anything, more bubbles may have been present in their study. Their pictures were re-analyzed in the current study, leading to the same results. We can only speculate on the possible explanations for this. For example, the bubbles imaged by Salter et al. (2014) may have been slightly smaller than those of the current study and therefore outside the range of detection.

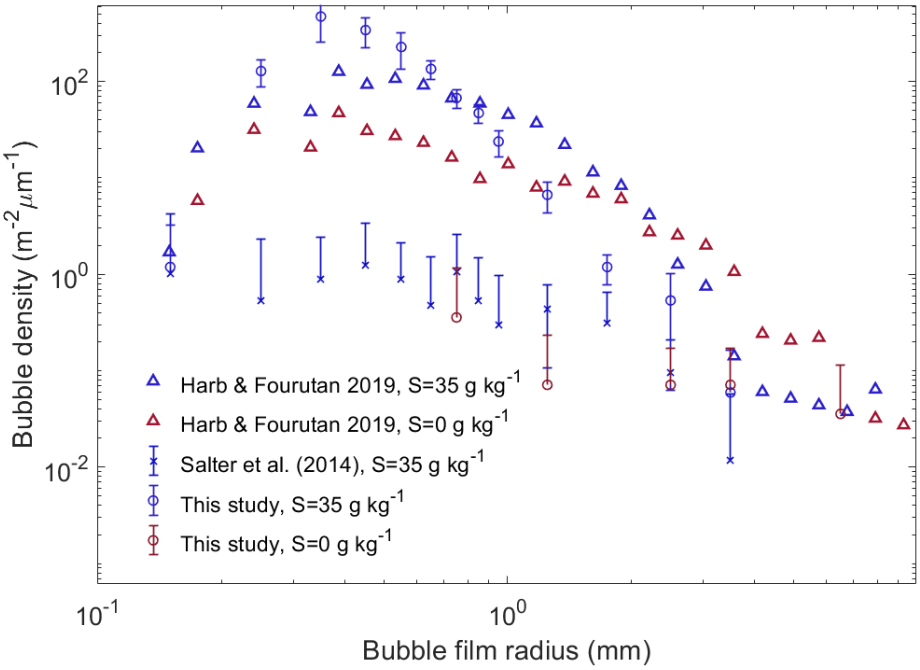

Figure 5. Comparison of bubble densities at salinities 0 and 35 g kg^{-1} with data from Harb and Foroutan (2019) and Salter et al. (2014). Values in panel (a) and (b) are presented as mean values and standard deviation. Error bars in panel (c) denote propagated standard errors.

3.3 Temperature dependence of particle production at three distinct salinities

Temperature ramps were conducted at salinities of 35 g kg^{-1}, 17 g kg^{-1} and 6 g kg^{-1} (Figure S6). Since we have previously conducted a temperature ramp at a salinity of 35 g kg^{-1} we were able to compare these two experiments for consistency. To do so we have used the Kolmogorov-Smirnov test to compare the integrated particle number, surface and volume concentrations as well as the effective radii at each temperature of these two temperature ramps. The integrated particle number concentrations and effective radii were found to have the same distribution with temperature at probability values of p=0.48 and p=0.34 (at a significance level of 5%), respectively. It is worth noting that the integrated number concentrations for both experiments were almost identical for temperatures ≥ 14°C, while they differed slightly at lower temperatures. The surface and volume concentrations were found to be different (p=2.6·10^{-4} and p=2.7·10^{-3} at a significance level of 5%, respectively). The change in sea spray particle number with water temperature (decreasing with increasing temperature) agrees qualitatively with many earlier studies (e.g. Bowyer et al., 1990; Mårtensson et al., 2003; Hultin et al., 2011; Zábori et al., 2012; Salter et al., 2014, 2015). We note that the difference between dN/dT for the 17 and 35 g kg^{-1} experiments is small, while the 6 g kg^{-1} experiment has a significantly smaller amplitude in dN/dT. Salter et al. (2014) concluded that it was changes to the bubble size distribution that were driving changes to particle production at seawater temperatures around ~ 10°C. In a similar fashion the data generated during the current study suggest that it is changes to the bubble spectra, especially the ratio between bubbles with radii larger than 1 mm and bubbles with radii smaller than 1 mm, that are driving changes to the particle size and number as salinity changes (see Figures 3 and 4c). However, the fact that the experiment at $S = 6$ g kg^{-1} exhibits the weakest trend in number concentration with water temperature suggests that

the temperature effect might be proportionally smaller at salinities representative for large parts of the Baltic Sea than it is for high salinity oceans.

3.3.1 Particle number and effective radius as a function of temperature and salinity

We have attempted to derive a parameterization of the particle number and effective radius as a function of temperature and salinity.

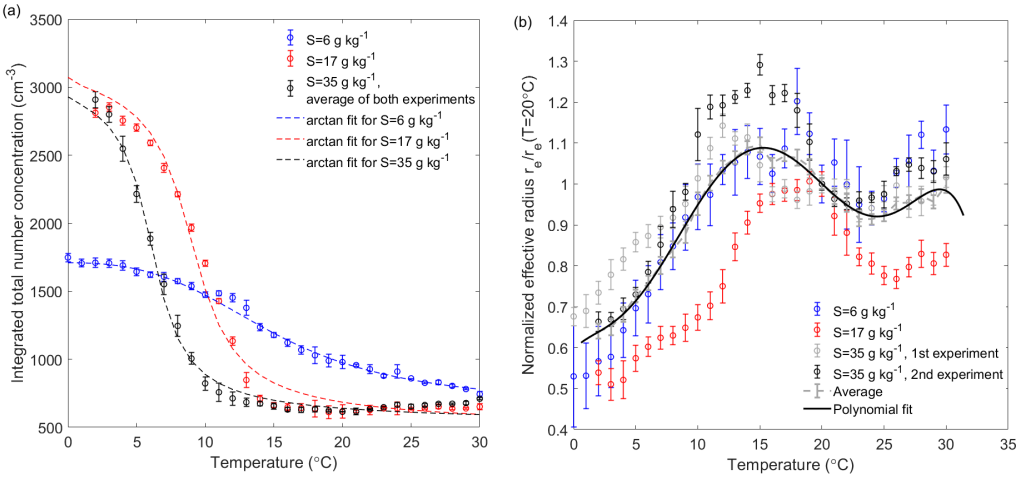

Figure 6. Effect of temperature on (a) integrated particle number for three different salinities with three fitted empirical equations and (b) effective radius normalized by the mean effective radius of the three salinities. The values in panel (a) are presented as mean values and standard deviation, while values in panel (b) are normalized to the value at T=20°C with propagated error bars.

The dependence of total particle number concentration on water temperature could be described with an equation building on the inverse tangent function (arctan) with correlation coefficients of $r^2 \geq 0.99$ for all three salinities (see also Figure 6a):

$$N_p = \int_{D,min}^{D,max} \frac{\mathrm{d}N}{\mathrm{dlogD_p}} d\log D_p = a - b \cdot \arctan\left(\frac{c(T^d) - e}{f}\right) \tag{6}$$

where N_p is the number concentration integrated over the whole size range (D, min = 0.015 µm and D, max = 10 µm in this study), T is the water temperature and the coefficients a to f are given in Table 1.

By normalizing the r_e with $r_e(T = 20°\mathrm{C})$ for each salinity experiment, we observe notable agreement between the experiments (see Figure 6b). By averaging the curves for the three salinities we were able to make a polynomial fit through the mean curve to produce r_e as function of T:

$$r_e = r_e(20°C) \cdot \sum_{i=1}^{n} \beta_i \cdot T^i. \tag{7}$$

The coefficients β_i are given in Table 2.

Table 1. Coefficients a to f for the parameterization of the number concentration for three different seawater salinities (see equation 6) as shown in Figure 6a, as well as the coefficient of determination, r^2.

S ($g\,kg^{-1}$)	a	b	c	d	e	f	r^2
6	1800	-734	17.4	2.467	$-1.7794 \cdot 10^3$	$-1.434 \cdot 10^4$	0.9958
17	1800	859.2	$6.674 \cdot 10^5$	0.3561	$1.47 \cdot 10^6$	$1.309 \cdot 10^5$	0.9882
35	1800	820	$-2.342 \cdot 10^4$	0.6871	-81700	$-1.595 \cdot 10^4$	0.9921

Table 2. Coefficients for the parameterization of the effective radius (equation 7) as shown in Figure 6b.

	Coefficients for eq. 7
β_0	0.596
β_1	$3.022 \cdot 10^{-2}$
β_2	$-8.178 \cdot 10^{-3}$
β_3	$2.109 \cdot 10^{-3}$
β_4	$-1.754 \cdot 10^{-4}$
β_5	$5.801 \cdot 10^{-6}$
β_6	$-6.72 \cdot 10^{-8}$

Now through combination of equation 7 with equation 4, which is valid at $T = 20°C$, we obtain

$$r_e = \alpha \cdot S^{1/3} = r_e(20°C) \cdot \sum_{i=1}^{n} \beta_i \cdot T^i \tag{8}$$

which provides the effective radius as a function of both S and T from 0-35 $g\,kg^{-1}$ and 0-30°C, respectively. In combination with equation 6 we have generated a simple parameterization of the sea spray particle number and effective radius as function of both water temperature and salinity assuming that one wishes to represent sea spray aerosol using a single mode. That however offers a less detailed parameterization than for example Mårtensson et al. (2003) or Salter et al. (2015).

4 Summary and conclusions

In this study we have performed a series of laboratory experiments to investigate the role of salinity on particle production and bubble spectra using a continuous plunging jet. We were able to describe the changes in particle number, volume and effective radius with salinity and identified three distinct salinity regimes in the particle number production. For salinities between 10 and 35 $g\,kg^{-1}$, the produced particle number was nearly constant. Between salinities 5 and 10 $g\,kg^{-1}$ we observed a local maximum in particle number concentration that coincided with a transition in the surface bubble spectra toward larger bubble sizes and decreased bubble density at lower salinities. Below 5 $g\,kg^{-1}$ we observed a rapid decrease in particle number, but only a gradual decrease in particle volume. Above salinity 5 $g\,kg^{-1}$ this decrease in volume with decreasing salinity was considerably steeper. Furthermore, we have observed a shift of the particle mode centered at 140 nm to $\sim$ 70 nm and a decrease in particles $>$ 200 nm as the salinity was decreased below 15 $g\,kg^{-1}$. The observed shift to smaller particles with decreasing salinity is attributed to the linear relationship between salinity and dry particle volume and the cubic relationship between salinity and effective radius. Changes in the particle production were further associated with changes in the surface bubble spectrum that exhibited higher numbers of bubbles with radii $<$1 mm

at higher salinities, while the number of droplets produced per bubble peaked at salinities below 5 $\mathrm{g\,kg^{-1}}$. Additionally, temperature ramps were conducted at three distinct salinities (35, 17 and 6 $\mathrm{g\,kg^{-1}}$). In terms of aerosol production, the experiments conducted at salinity 35 $\mathrm{g\,kg^{-1}}$ and 17 $\mathrm{g\,kg^{-1}}$ did not differ markedly and exhibit a similar $\mathrm{d}N/\mathrm{d}T$ trend to Bowyer et al. (1990), Mårtensson et al. (2003), Hultin et al. (2011), Zábori et al. (2012) and Salter et al. (2014, 2015). Salter et al. (2014) explained this temperature trend with a shift in the surface water bubble population with changing temperature. The temperature ramp at $S = 6\,\mathrm{g\,kg^{-1}}$ exhibited aerosol production that was qualitatively similar to the 17 and 35 $\mathrm{g\,kg^{-1}}$ ramps, but with a weaker amplitude (smaller $\mathrm{d}N/\mathrm{d}T$ values). It may be that the two different processes both mediated through changes in bubble population by either changes in temperature or salinity interfere with each other for low salinity waters. Finally, we have derived a simple sea spray source parameterization of particle number and particle effective radius as function of salinity and water temperature based on the observed relationships that can be used to model the impact of salinity on sea spray production.

5 Acknowledgments

This work was supported by the Swedish Research Council (VR): "Characterising properties of Climate Relevant Organic and Inorganic Sea-Spray-aerosols, Sources and Air-sea exchange causing their Net-emission" (CROISSANT, project no. 2018-04255), as well as several previous VR-grants that has financed the sea spray simulation tank with its aerosol and water instrumentation. In addition we wish to express our gratitude to the Bolin Climate Centre for supporting part of the aerosol instrumentation. P.Z. was supported by the Vetenskapsrådet starting grant, project no. 2018-05045 and M.E.S was supported by Vetenskapsrådet project no. 2016-05100. A special thanks is extended to Piotr Markuszewski and Gabriel Pereira Freitas for fruitful discussions.

The data of this study are available on the Bolin Centre for Climate Research Database (https://doi.org/10.17043/zinke-2021-laboratory-1).

References

Abo Riziq, A., Erlick, C., Dinar, E., & Rudich, Y. (2007). Optical properties of absorbing and non-absorbing aerosols retrieved by cavity ring down (CRD) spectroscopy. *Atmospheric Chemistry and Physics*, *7*(6), 1523–1536. doi: 10.5194/acp-7-1523-2007

Asher, W., Karle, L., & Higgins, B. (1997). On the differences between bubble-mediated air-water transfer in freshwater and seawater. *Journal of Marine Research*, *55*(5), 813–845.

Bowyer, P. A., Woolf, D. K., & Monahan, E. C. (1990). Temperature dependence of the charge and aerosol production associated with a breaking wave in a whitecap simulation tank. *Journal of Geophysical Research: Oceans*, *95*, 5313–5319. doi: 10.1029/JC095iC04p05313

Carey, W. M., Fitzgerald, J. W., Monahan, E. C., & Wang, Q. (1993). Measurement of the sound produced by a tipping trough with fresh and salt water. *The Journal of the Acoustical Society of America*, *93*(6), 3178–3192.

Cartmill, J. W., & Su, M. Y. (1993). Bubble size distribution under saltwater and freshwater breaking waves. *Dynamics of atmospheres and oceans*, *20*(1-2), 25–31.

Collins, D. B., Zhao, D. F., Ruppel, M. J., Laskina, O., Grandquist, J. R., Modini, R. L., ... Prather, K. A. (2014). Direct aerosol chemical composition measurements to evaluate the physicochemical differences between controlled sea spray aerosol generation schemes. *Atmospheric Measurement Techniques*, *7*, 3667-3683.

Craig, V. S. J., Ninham, B. W., & Pashley, R. M. (1993). The effect of electrolytes on bubble coalescence in water. *J. Phys. Chem.*, *97*, 10192–10197.

Drogaris, G., & Weiland, P. (1983). Coalescence behaviour of gas bubbles in aqueous solutions of n-alcohols and fatty acids. *Chemical engineering science*, *38*(9), 1501–1506.

Facchini, M. C., Rinaldi, M., Decesari, S., Carbone, C., Finessi, E., Mircea, M., ... O'Dowd, C. D. (2008). Primary submicron marine aerosol dominated by insoluble organic colloids and aggregates. *Geophys. Res. Lett.*, *35*. doi: 10.1029/2008GL034210

Grainger, R., Lambert, A., Rodgers, C., Taylor, F., & Deshler, T. (1995). Stratospheric aerosol effective radius, surface area and volume estimated from infrared measurements. *Journal of Geophysical Research: Atmospheres*, *100*(D8), 16507–16518.

Harb, C., & Foroutan, H. (2019). A systematic analysis of the salinity effect on air bubbles evolution: Laboratory experiments in a breaking wave analog. *Journal of Geophysical Research: Oceans*, *124*(11), 7355–7374.

Hultin, K. A. H., Krejci, R., Pinhassi, J., Gomez-Consarnau, L., Mårtensson, E. M., Hagström, A., & Nilsson, E. D. (2011). Aerosol and bacterial emissions from Baltic seawater. *Atmospheric Research*, *99*, 1–14. doi: 10.1016/j.atmosres.2010.08.018

Hultin, K. A. H., Nilsson, E. D., Krejci, R., Mårtensson, M., E. M. Ehn, Hagström, A., & de Leeuw, G. (2010). In situ laboratory sea spray production during the Marine Aerosol Production 2006 cruise on the northeastern Atlantic Ocean. *Journal of Geophysical Research: Atmospheres*, *115*. doi: 10.1029/2009JD012522

Katsir, Y., Goldstein, G., & Marmur, A. (2015). Bubble the wave or waive the bubble: Why seawater waves foam and freshwater waves do not? *Colloid and Interface Science Communications*, *6*, 9–12.

Kniebusch, M., Meier, H. M., & Radtke, H. (2019). Changing salinity gradients in the baltic sea as a consequence of altered freshwater budgets. *Geophysical Research Letters*, *46*(16), 9739–9747.

Lavoie, D., Lambert, N., & Van der Baaren, A. (2013). Projections of future physical and biogeochemical conditions in Hudson and Baffin bays from CMIP5 global climate models. *Canadian Technical Report of Hydrography and Ocean Sciences 289*.

Lessard, R. R., & Zieminski, S. A. (1971). Bubble coalescence and gas transfer in aquaeous electrolyte solutions. *Industrial and Engineering Chemistry. Fundamentals*, *19*, 260–269.

Lewis, E. R., & Schwartz, S. E. (2004). *Sea salt aerosol production: Mechanisms, methods, measurements and models - A critical review.* Geophysical Monograph Series, Vol.

152, American Geophysical Union,.

Mårtensson, E. M., Nilsson, E. D., de Leeuw, G., Cohen, L. H., & Hansson, H. C. (2003). Laboratory simulations and parameterization of the primary marine aerosol production. *Journal of Geophysical Research: Atmospheres*, *108*. doi: 10.1029/2002JD002263

Marrucci, G., & Nicodemo, L. (1967). Coalescence of gas bubbles in aqueous solutions of inorganic electrolytes. *Chemical Engineering Science*, *22*(9), 1257–1265.

May, N. W., Axson, J. L., Watson, A., Pratt, K. A., & Ault, A. P. (2016). Lake spray aerosol generation: A method for producing representative particles from freshwater wave breaking. *Atmospheric Measurement Techniques*, *2016*, 1–38. doi: 10.5194/amt-2016-115

Monahan, E. C., & Zietlow, C. R. (1969). Laboratory comparisons of fresh-water and salt-water whitecaps. *Journal of Geophysical Research*, *74*(28), 6961–6966.

Murphy, D., Anderson, J., Quinn, P., McInnes, L., Brechtel, F., Kreidenweis, S., ... Buseck, P. (1998). Influence of sea-salt on aerosol radiative properties in the Southern Ocean marine boundary layer. *Nature*, *392*(6671), 62–65.

Nilsson, E. D., Hultin, K. A., Mårtensson, E. M., Markuszewski, P., Rosman, K., & Krejci, R. (2021). Baltic sea spray emissions: In situ eddy covariance fluxes vs. simulated tank sea spray. *Atmosphere*, *12*(2), 274.

Park, J. Y., Lim, S., & Park, K. (2014). Mixing state of submicrometer sea spray particles enriched by insoluble species in bubble-bursting experiments. *Journal of Atmospheric and Oceanic Technology*, *31*(1), 93–104.

Quinn, P., Coffman, D., Kapustin, V., Bates, T., & Covert, D. (1998). Aerosol optical properties in the marine boundary layer during the first aerosol characterization experiment (ACE 1) and the underlying chemical and physical aerosol properties. *Journal of Geophysical Research: Atmospheres*, *103*(D13), 16547–16563.

Salter, M. E., Hamacher-Barth, E., Leck, C., Werner, J., Johnson, C. M., Riipinen, I., ... Zieger, P. (2016). Calcium enrichment in sea spray aerosol particles. *Geophysical Research Letters*, *43*(15), 8277–8285.

Salter, M. E., Nilsson, E. D., Butcher, A., & Merete, B. (2014). On the seawater temperature dependence of continuous plunging jet derived sea spray aerosol. *Journal of Geophysical Research: Atmospheres*. doi: 10.1002/2013JD021376

Salter, M. E., Zieger, P., Acosta Navarro, J. C., Grythe, H., Kirkevåg, A., Rosati, B., ... Nilsson, E. D. (2015). An empirically derived inorganic sea spray source function incorporating sea surface temperature. *Atmospheric Chemistry and Physics*, *15*(19), 11047–11066. doi: 10.5194/acp-15-11047-2015

Schwartz, S. E. (1996). The whitehouse effect—shortwave radiative forcing of climate by anthropogenic aerosols: An overview. *Journal of Aerosol Science*, *27*(3), 359–382.

Slade, J., VanReken, T., Mwaniki, G., Bertman, S., Stirm, B., & Shepson, P. (2010). Aerosol production from the surface of the Great Lakes. *Geophysical Research Letters*, *37*(18).

Slauenwhite, D. E., & Johnson, B. D. (1999). Bubble shattering: Differences in bubble formation in fresh water and seawater. *Journal of Geophysical Research: Oceans*, *104*, 3265–3275.

Stokes, M. D., Deane, G. B., Prather, K., Bertram, T. H., Ruppel, M. J., Ryder, O. S., ... Zhao, D. (2013). A marine aerosol reference tank system as a breaking wave analogue for the production of foam and sea-spray aerosols. *Atmospheric Measurement Techniques*, *6*(4), 1085–1094. Retrieved from `http://www.atmos-meas-tech.net/6/1085/2013/` doi: 10.5194/amt-6-1085-2013

Tyree, C. A., Hellion, V. M., Alexandrova, O. A., & Allen, J. O. (2007). Foam droplets generated from natural and artificial seawaters. *Journal of Geophysical Research: Atmospheres*, *112*. doi: 10.1029/2006JD007729

von der Weiden, S. L., Drewnick, F., & Borrman, S. (2009). Particle loss calculator - a new software tool for the assessment of the performance of aerosol inlet systems. *Atmospheric Measurement Techniques*, *2*, 479–494.

Wang, X., Deane, G. B., Moore, K. A., Ryder, O. S., Stokes, M. D., Beall, C. M., ... others

(2017). The role of jet and film drops in controlling the mixing state of submicron sea spray aerosol particles. *Proceedings of the National Academy of Sciences*, *114*(27), 6978–6983.

Zábori, J., Matisāns, M., Krejci, R., Nilsson, E. D., & Ström, J. (2012). Artificial primary marine aerosol production: a laboratory study with varying water temperature, salinity and succinic acid concentration. *Atmospheric Chemistry and Physics*, *12*, 10709–10724. doi: 10.5194/acp-12-10709-2012

Zieger, P., Väisänen, O., Corbin, J. C., Partridge, D. G., Bastelberger, S., Mousavi-Fard, M., ... others (2017). Revising the hygroscopicity of inorganic sea salt particles. *Nature Communications*, *8*(1), 1–10.

Figure 1.

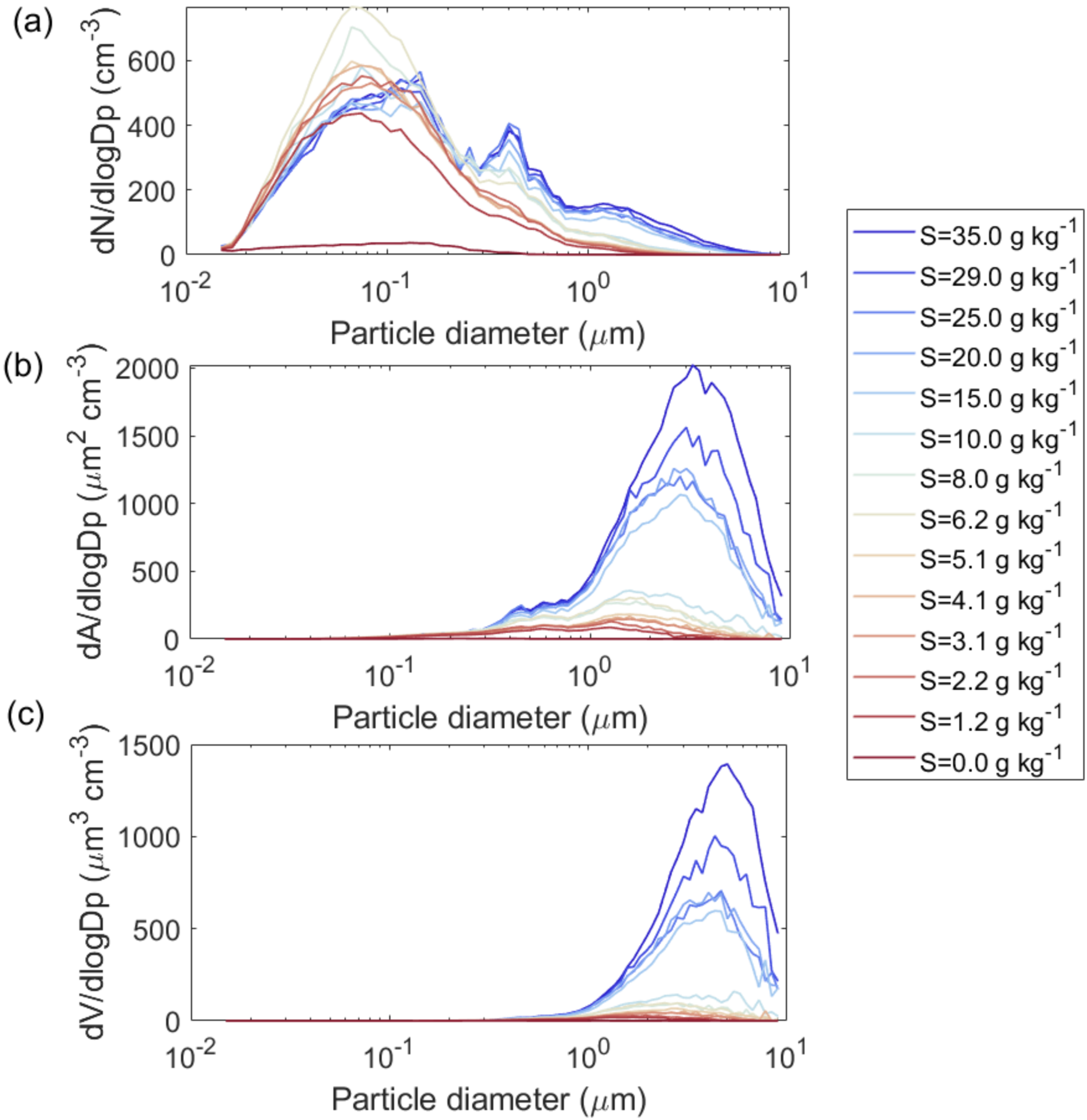
(a)
dN/dlogDp (cm-3)
600
400
200
0
10-2
10-1
100
101
Particle diameter (μm)
(b)
dA/dlogDp (μm2 cm-3)
2000
1500
1000
500
0
10-2
10-1
100
101
Particle diameter (μm)
(c)
dV/dlogDp (μm3 cm-3)
1500
1000
500
0
10-2
10-1
100
101
Particle diameter (μm)
S=35.0 g kg-1
S=29.0 g kg-1
S=25.0 g kg-1
S=20.0 g kg-1
S=15.0 g kg-1
S=10.0 g kg-1
S=8.0 g kg-1
S=6.2 g kg-1
S=5.1 g kg-1
S=4.1 g kg-1
S=3.1 g kg-1
S=2.2 g kg-1
S=1.2 g kg-1
S=0.0 g kg-1

Figure 2.

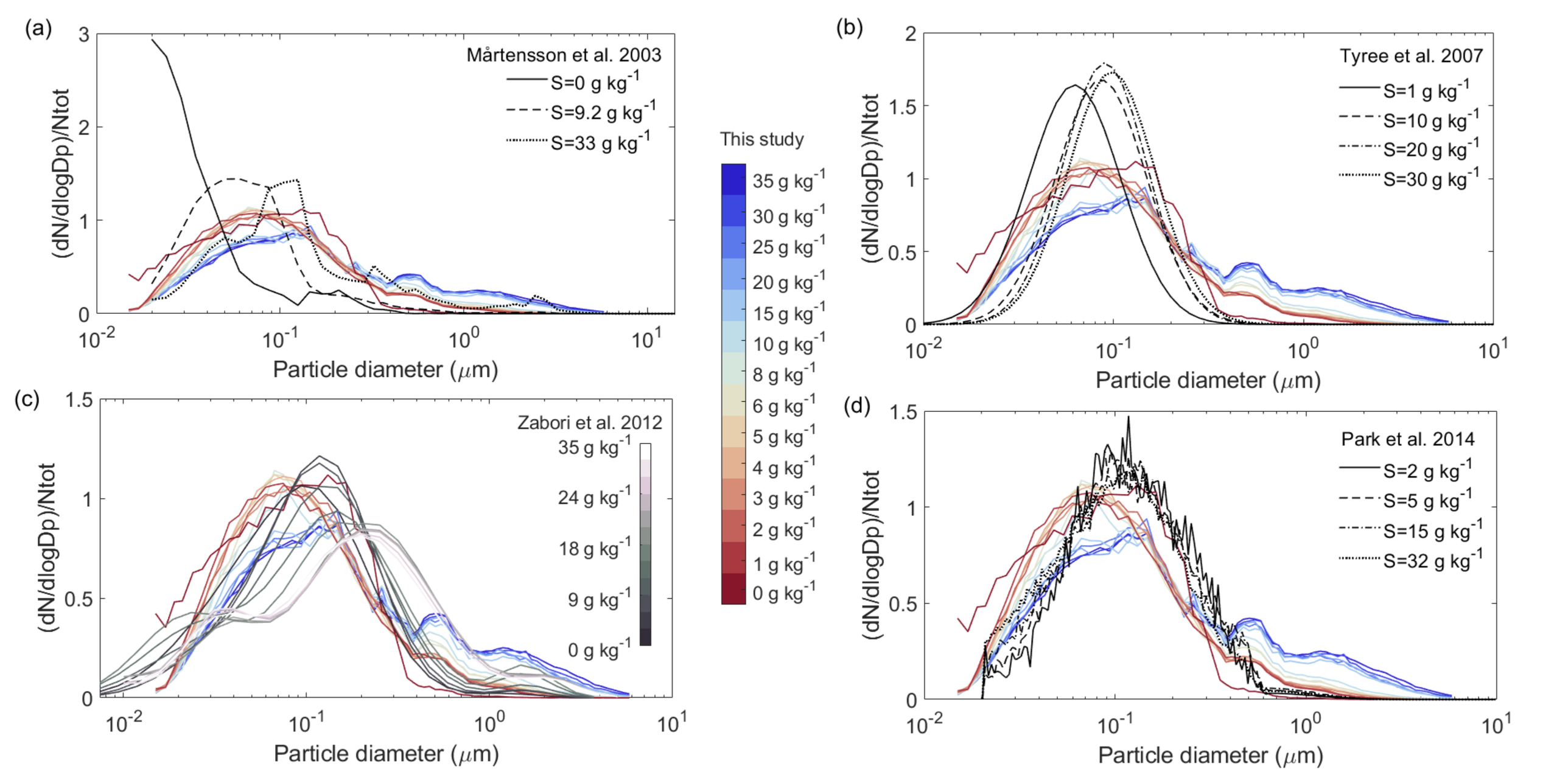
(a)
Mårtensson et al. 2003
S=0 g kg-1
S=9.2 g kg-1
S=33 g kg-1
(dN/dlogDp)/Ntot
Particle diameter (μm)
(b)
Tyree et al. 2007
S=1 g kg-1
S=10 g kg-1
S=20 g kg-1
S=30 g kg-1
(dN/dlogDp)/Ntot
Particle diameter (μm)
This study
35 g kg-1
30 g kg-1
25 g kg-1
20 g kg-1
15 g kg-1
10 g kg-1
8 g kg-1
6 g kg-1
5 g kg-1
4 g kg-1
3 g kg-1
2 g kg-1
1 g kg-1
0 g kg-1
(c)
Zabori et al. 2012
35 g kg-1
24 g kg-1
18 g kg-1
9 g kg-1
0 g kg-1
(dN/dlogDp)/Ntot
Particle diameter (μm)
(d)
Park et al. 2014
S=2 g kg-1
S=5 g kg-1
S=15 g kg-1
S=32 g kg-1
(dN/dlogDp)/Ntot
Particle diameter (μm)

Figure 3.

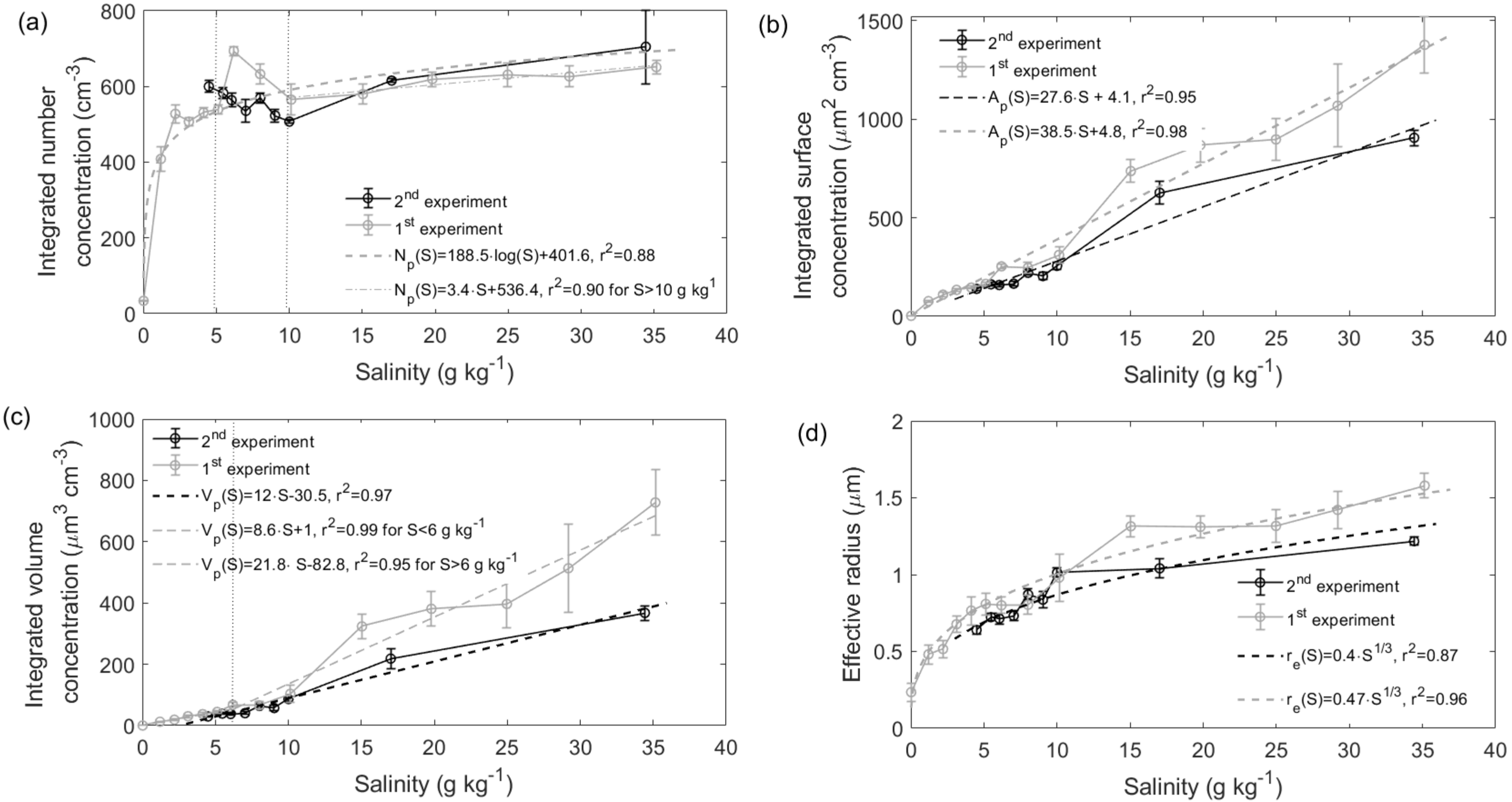
(a)
Integrated number concentration (cm^{-3})
Salinity (g kg^{-1})
2nd experiment
1st experiment
$N_p(S)=188.5\cdot\log(S)+401.6$, $r^2=0.88$
$N_p(S)=3.4\cdot S+536.4$, $r^2=0.90$ for S>10 g kg^{-1}
(b)
Integrated surface concentration (μm^2 cm^{-3})
Salinity (g kg^{-1})
2nd experiment
1st experiment
$A_p(S)=27.6\cdot S + 4.1$, $r^2=0.95$
$A_p(S)=38.5\cdot S+4.8$, $r^2=0.98$
(c)
Integrated volume concentration (μm^3 cm^{-3})
Salinity (g kg^{-1})
2nd experiment
1st experiment
$V_p(S)=12\cdot S-30.5$, $r^2=0.97$
$V_p(S)=8.6\cdot S+1$, $r^2=0.99$ for S<6 g kg^{-1}
$V_p(S)=21.8\cdot S-82.8$, $r^2=0.95$ for S>6 g kg^{-1}
(d)
Effective radius (μm)
Salinity (g kg^{-1})
2nd experiment
1st experiment
$r_e(S)=0.4\cdot S^{1/3}$, $r^2=0.87$
$r_e(S)=0.47\cdot S^{1/3}$, $r^2=0.96$

Figure 4.

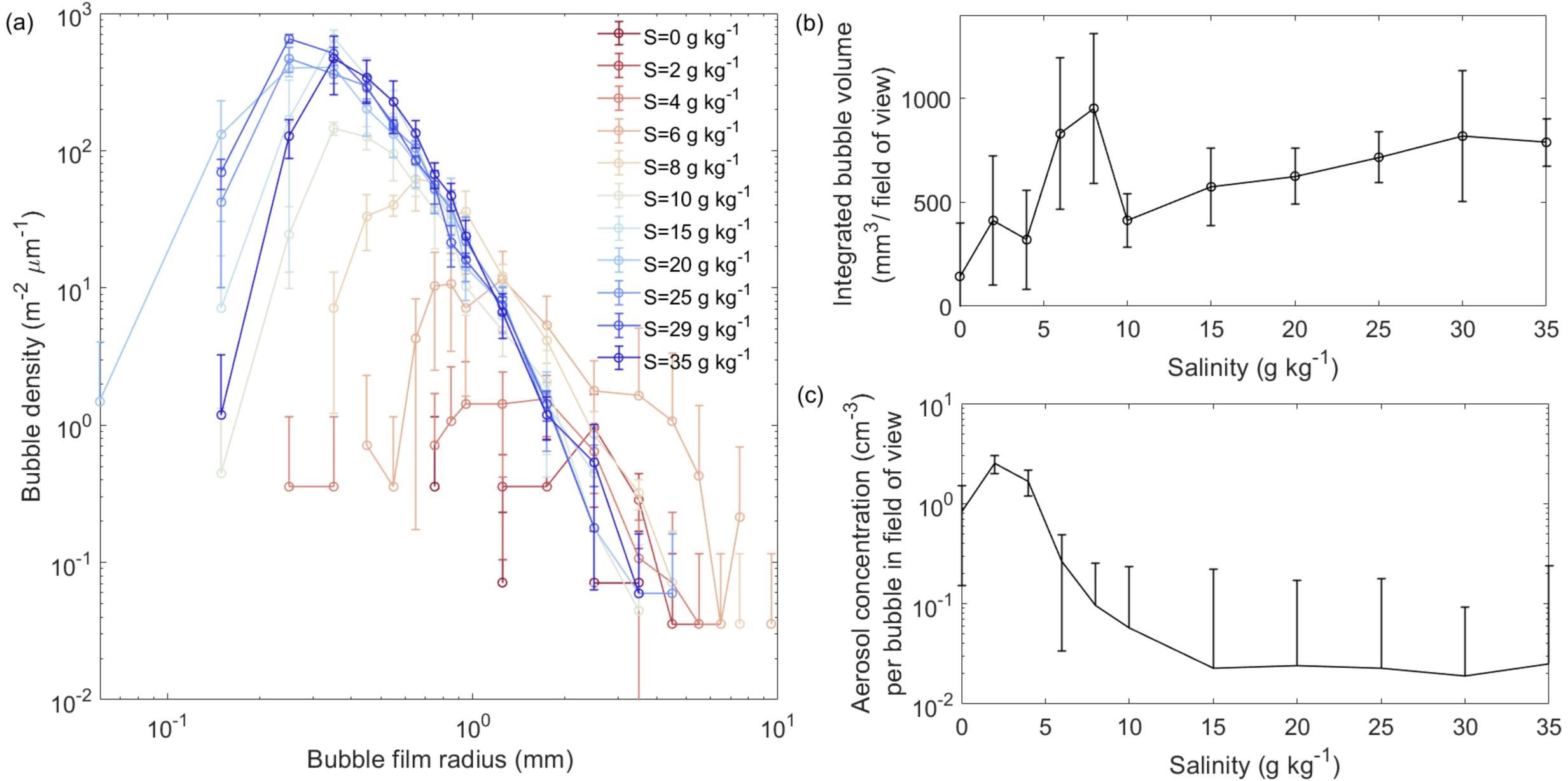
(a)
Bubble density (m^{-2} μm^{-1})
Bubble film radius (mm)
S=0 g kg^{-1}
S=2 g kg^{-1}
S=4 g kg^{-1}
S=6 g kg^{-1}
S=8 g kg^{-1}
S=10 g kg^{-1}
S=15 g kg^{-1}
S=20 g kg^{-1}
S=25 g kg^{-1}
S=29 g kg^{-1}
S=35 g kg^{-1}
(b)
Integrated bubble volume (mm^3/ field of view)
Salinity (g kg^{-1})
(c)
Aerosol concentration (cm^{-3}) per bubble in field of view
Salinity (g kg^{-1})

Figure 5.

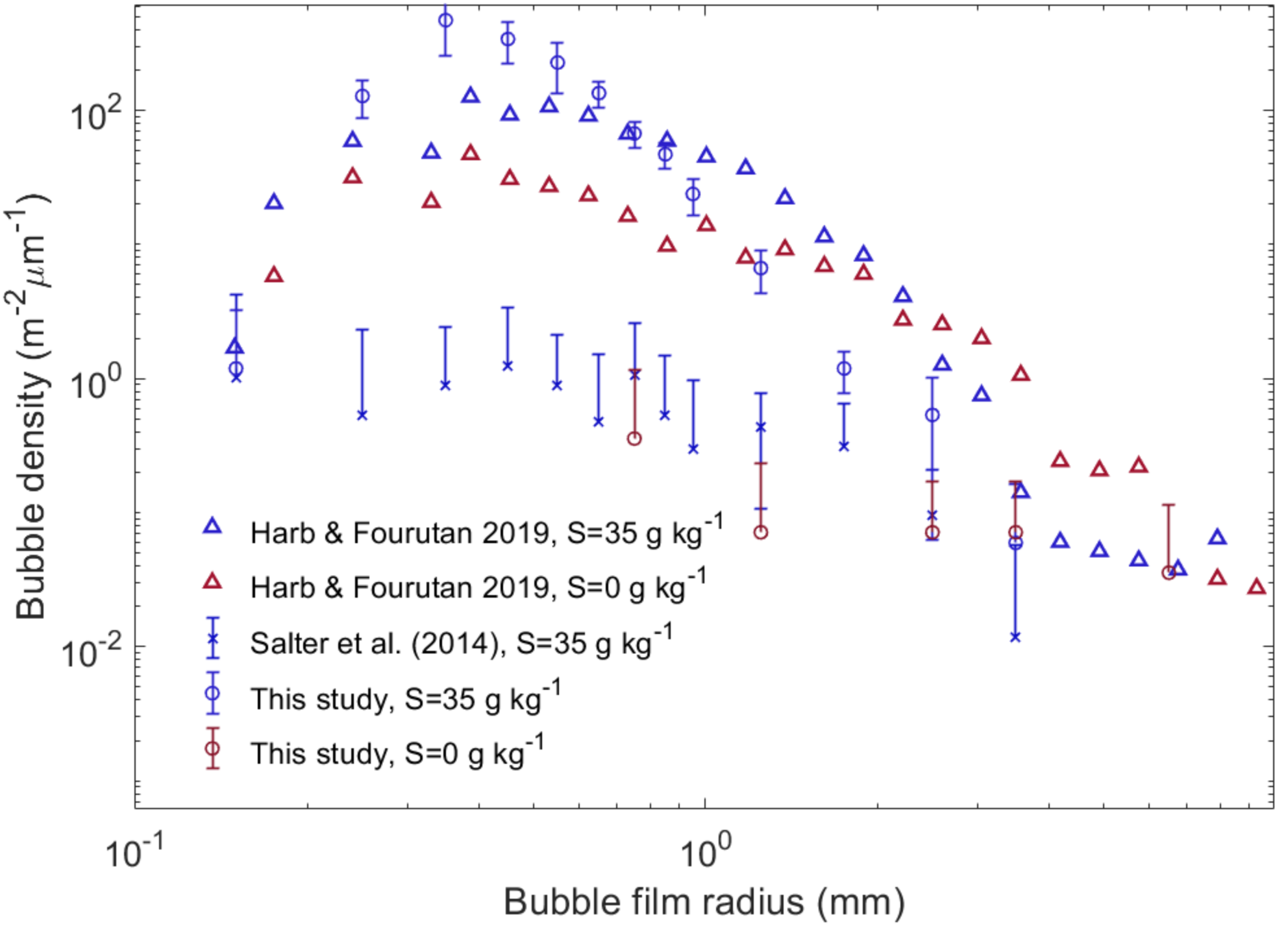
Bubble density ($m^{-2} \mu m^{-1}$)
10^2
10^0
10^{-2}
10^{-1}
10^0
Bubble film radius (mm)
Harb & Fourutan 2019, S=35 g kg^{-1}
Harb & Fourutan 2019, S=0 g kg^{-1}
Salter et al. (2014), S=35 g kg^{-1}
This study, S=35 g kg^{-1}
This study, S=0 g kg^{-1}

Figure 6.

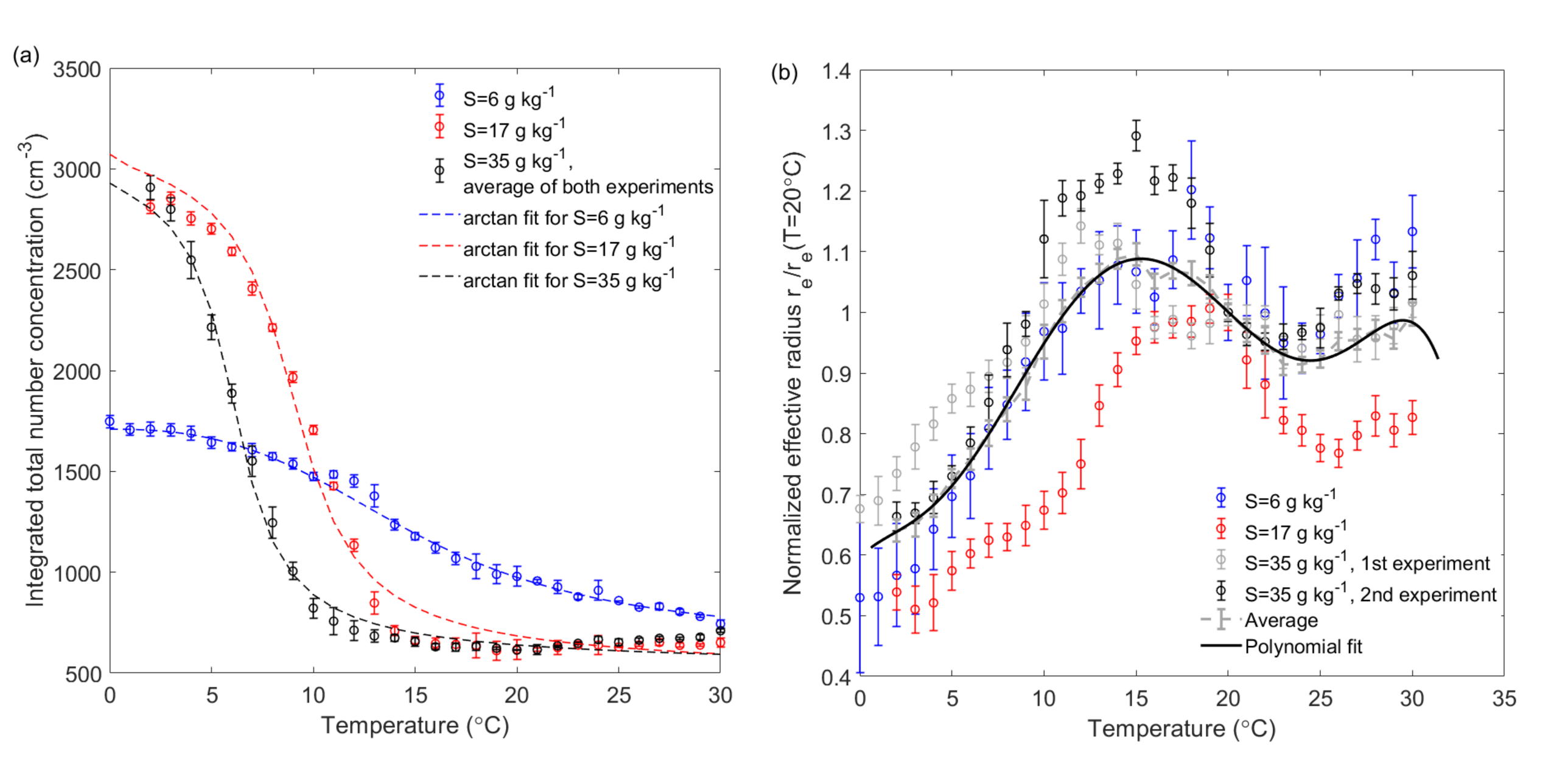
(a)
Integrated total number concentration (cm^{-3})
Temperature (°C)
S=6 g kg^{-1}
S=17 g kg^{-1}
S=35 g kg^{-1}, average of both experiments
arctan fit for S=6 g kg^{-1}
arctan fit for S=17 g kg^{-1}
arctan fit for S=35 g kg^{-1}
(b)
Normalized effective radius r_e/r_e(T=20°C)
Temperature (°C)
S=6 g kg^{-1}
S=17 g kg^{-1}
S=35 g kg^{-1}, 1st experiment
S=35 g kg^{-1}, 2nd experiment
Average
Polynomial fit